Arabian Journal of Chemistry (2022) **15**, 103713

King Saud University

**Arabian Journal of Chemistry**

www.ksu.edu.sa
www.sciencedirect.com

ORIGINAL ARTICLE

# Cervical cancer treatment of Co(II) coordination polymer through miR-9-5p-regulated BRCA1-OCT1-GADD45 pathways



**Xia Zhao, Wei-Lei Dong, Gui-Fang Luo, Jing Xie, Ji Liu, Fu-Rong Yu**

*Department of Gynaecology and Obstetrics, The First Affiliated Hospital, University of South China, Hengyang, Hunan, China*

Received 1 October 2021; accepted 16 January 2022
Available online 20 January 2022

**KEYWORDS**

Coordination polymer;
Cervical cancer;
microRNA;
miR-9-5p;
BRCA1

**Abstract** Fresh Co(II) coordinating coordination polymer based on {[Co(μ-ppda)(μ-pbmeix)]•0.5pbmeix·$H_2O$}$_n$ (1) was formed smoothly through the reaction of Co(II) salt with *p*-phenylenediacetic acid ($H_2$ppda) under the conditions of N-donor co-ligand semirigid 1,4-bis(2-methylimidazol-1-ylmethyl)benzene (pbmeix) for cervical cancer therapy. In our biological research, we explored the pathogenesis of cervical cancer and provided new targets for cervical cancer treatment. In patients with cervical cancer and the cervical cancer rat model, the expression of Breast Cancer Susceptibility Protein-1 (BRCA1) was aberrantly upregulated. This phenomenon may play a role in the occurrence and development of cervical cancer. Then, bioinformatics prediction was conducted, and miR-9-5p was speculated as the up-regulator of BRCA1 in cervical cancer cells. The influence of miR-9-5p on the vascular endothelial growth factor and pigment epithelium-derived factor contents of cervical cancer lesions was determined via enzyme-linked immunosorbent (ELISA) assay. Then, the proliferation of cervical cancer cells was determined via CCK-8 assay after miR-9-5p transfection. Finally, we proved that complex **1** is an excellent candidate for cervical cancer therapy through miR-9-5p-regulated BRCA1-OCT1-GADD45 pathways.



## 1. Introduction

Cervical cancer is the second most common malignancy after breast cancer in women worldwide (Wuerthner and Avila-Wallace, 2016). According to worldwide statistics, there are about 500,000 new cases of cervical cancer each year, accounting for 5% of all new cancer cases, of which 80% are from developing countries (Fang et al., 2014; Tsikouras et al., 2016). However, the pathogenesis of cervical cancer is still unclear. Thus, research on the pathogenesis of cervical cancer and new targets for cervical cancer treatment is urgently necessary. BRCA1 is a suppressor gene directly implicated in hereditary breast cancer, which is also regarded as the target for the cancer therapy. The importance of the BRCA1 in the cervical cancer development was still need to be explored.

E-mail address: feiweiyan6678367@163.com (F.-R. Yu)

Peer review under responsibility of King Saud University.

Production and hosting by Elsevier

https://doi.org/10.1016/j.arabjc.2022.103713
1878-5352 © 2022 The Authors. Published by Elsevier B.V. on behalf of King Saud University.

In recent years, Breast Cancer Susceptibility Protein-1 (BRCA1) has been reported to be related to a variety of biological processes, such as cell viability, adhesion, and membrane fluidity. A significant change in BRCA1 expression level has also been detected in different cancer disease lesions (Harao et al., 2018; Xu et al., 2018). Nevertheless, whether BRCA1 also participates in the pathogenesis of cervical cancer remains to be confirmed. Thus, increasing BRCA1 expression in cervical cancer lesions and identifying the specific regulatory mechanism was realized in the current study.

MicroRNA (miRNA) comprises a class of small (20 to 24 nucleotides) noncoding RNA that is related to the negative posttranscriptional regulation of genetic expression in multicellular organisms via fractional or whole complimentary matching with the three prime untranslated region (3′-UTR) of target messenger RNA (mRNA), influencing the translation and constancy of mRNA and adjusting different types of cell functions (Amini et al., 2019). In the past decades, an increasing number of studies have shown that miRNA plays a momentous role in the origin and growth of cervical cancer (Laengsri et al., 2018; Shen et al., 2020). However, whether other types of miRNA are related to the angiogenesis procedure in cervical cancer requires further exploration. Such research may be a promising target for the diagnosis and therapy of cervical cancer.

The design and creation of coordination polymers (CPs) have elicited considerable attention because of their potential extensive applications to functional materials. The structures and properties of CPs originate from multiple molecular building blocks linked by coordinate bonds and m[illegible] molecule catenation (Liu et al., 2018; Raja et al., 2012; Hu et al., 2015). In the present research, a novel Co(II) complex was designed and synthesized by usi[illegible] mixe[illegible] ligand synthesis method. The as-prepared C[illegible] **1** wa[illegible] formed smoothly through various methods, such as X-r[illegible] single-crystal diffraction, infrared (IR) spectoscopy, thermogravimetric analysis (TGA), elemental analysis, a[illegible] powder X-ray diffraction (PXRD).

In our biological research, data from cervical cancer patients in our hospital we[illegible] collected a[illegible] a cervical cancer rat model was constructe[illegible] Reverse transcription polymerase chain reaction (RT-PCR) indicated an abnormal overexpression level of BRCA1 within cervical cancer lesions, demonstrating the important r[illegible] of BRCA[illegible] in the occurrence and development [illegible] cervical cancer. Subsequently, the results of the bioinformatics prediction showed that miR-9-5p may be a latent n[illegible]-type r[illegible] of BRCA1 expression and can bind to the 3′-UT[illegible] BRCA1. Furthermore, an in vivo study indicated that the restoration of miR-9-5p expression restrained BRCA1 expression and VEGF and PEDF contents in cervical cancer lesions. Moreover, analyses of molecular functions related to cervical cancer courses showed that miR-9-5p restrains the proliferation of cervical cancer cells via BRCA1-induced OCT1 and GADD45 pathway. Finally, we proved that complex **1** has excellent application values in cervical cancer therapy by regulating miR-9-5p relative expression. All the results of this research suggest that controlling the level of miR-9-5p/ BRCA1 may have major therapeutic significance for cervical cancer diseases.

## 2. Methods

### 2.1. Chemicals and measurements

All reagents met the quality standards for analysis and did not require further purification. The elements C, H, and N were analyzed. The IR spectrum was recorded on a TENSOR 27 spectrophotometer, with a range of 400–4000 $cm^{-1}$. Powder X-ray diffractograms were measured with a Bruker SMART D8 Advance X-ray diffractometer that applied Cu Kα radiation (λ was 1.5406 Å) at 40 kV and 30 mA. TGA results were obtained using a TGA/1100SF thermogravimetric analyzer.

The cervical cancer cells used in the experiment were acquired from the American Type Culture Collection (ATCC; Rockville, MD). The cells were cultivated in Dulbecco's modified Eagle's medium (Gibco, [illegible] USA) that was added to 10% fetal bovine serum (Thermo Fisher Scientific), 1% penicillin/streptomycin solution (Hyclone Laboratories, Logan, UT, USA), and 2% L-glutamine. All the cells were cultivated at 37 ℃ in a moist 5% $CO_2$ incubator.

### 2.2. Preparation and characterization of $\{[Co(\mu\text{-ppda})(\mu\text{-pbmeix})_{0.5}pbmeix\cdot H_2O\}_n$ (1)

To obtain the compound, 12 mL of dimethylformamide (DMF)/$H_2O$ (ratio was 4:1), 0.10 g of *p*-phenylenediacetic acid ($H_2$ppda), 0.1[illegible] g of $Co(NO_3)_2\cdot 6H_2O$, and 0.14 g of 1,4-bis(2-methylimidazol-1-ylmethyl)benzene (pbmeix) were mixed in a thick-walled glass tube. Then, the solution was kept at 120℃ for 72 h. After lowering to the normal temperature at a rate of [illegible] per hour, the solution was filtered and allowed to evaporate slowly. After several days, pink crystals were obtained through filtration and washing. Anal. Cald. for **1** ($C_{34}H_{35}CoN_6O_5$): the C content was 61.26%, the H content was 5.29%, and the N content was 12.61%. Found: the C content was 61.15%, the H content was 5.33%, and the N content was 12.74%.

A SuperNova diffractometer was utilized to collect X-ray data. The statistical analysis of diverse intensity figures was conducted through Crysalispro program, and the data were recorded in hkl pattern. The mode of SHELXS that used direct means was adopted to construct the fundamental framework, and the mode of SHELXL-2014 that used the least squares method was changed. Different inhomogeneous parameters were selected to refine non H atoms. Then, all the H atoms that applied AFIX software were tied to the C atoms. Table 1 provides the specific parameters of complex **1**.

### 2.3. Animal model construction

The 40 SD rats (6–8, 180–220 g) used in this study were obtained from the Experimental Animal Research Center (Zhejiang, China) and reared with free water and food. All the animals were kept in a standard environment before preformation. All the processes in this experiment were endorsed by the animal experiment ethics committee of the Animal Health Committee of Zhejiang University (Zhejiang, China). The cervical cancer rat model was constructed in accordance

**Table 1** Experimental details and crystallographic results of Mixture **1**.

| Empirical formula | $C_{34}H_{35}CoN_6O_5$ |
|---|---|
| Formula weight | 666.61 |
| Temperature/K | 293(2) |
| Crystal system | triclinic |
| Space group | P-1 |
| a/Å | 10.2217(3) |
| b/Å | 13.05270(10) |
| c/Å | 13.1782(2) |
| α/° | 106.231(3) |
| β/° | 108.8540(10) |
| γ/° | 100.6620(10) |
| Volume/Å$^3$ | 1522.47(6) |
| Z | 2 |
| $\rho_{calc}$g/cm$^3$ | 1.454 |
| μ/mm$^{-1}$ | 0.618 |
| Reflections collected | 15,327 |
| Independent reflections | 8184 [$R_{int}$ = 0.0240, $R_{sigma}$ = 0.0465] |
| Data/restraints/parameters | 8184/156/442 |
| Goodness-of-fit on $F^2$ | 1.068 |
| Final R indexes [I > =2σ (I)] | $R_1$ = 0.0537, ω$R_2$ = 0.1346 |
| Final R indexes [all data] | $R_1$ = 0.0685, ω$R_2$ = 0.1452 |
| Largest diff. peak/hole / e Å$^{-3}$ | 1.47/-0.59 |
| CCDC | 2,105,276 |

with the statement of the Association for Visual and Ophthalmic Research on the utilization of animals in ophthalmic and visual research (Castro et al., 2004). The animals were euthanized on the seventh day after treatment to assess BRCA1 mRNA level by using real-time RT-PCR (RT-qPCR).

### 2.4. RT-qPCR

The relative expression of BRCA1 or miR-9-5p in cervical cancer lesions or cervical cancer cells was measured through RT-qPCR. All operations during the experiment followed the manufacturer's instructions with several appropriate modifications (Qian et al., 2019). In summary, the total RNA in the cervical cancer lesions or cervical cancer cells was separated by applying Trizol (Thermo Fisher Scientific), followed by RNA qualification in NanoDrop 2000 (Qiawell, San Jose, CA, USA). Subsequently, 1000 ng of whole RNA was reverse-transcribed into complementary DNA (cDNA) via a reverse transcription kit (Takara, Dalian, China). RT-qPCR preformation was performed on an SYBR-Green Real-Time Master Mix (Roche), with the *gapdh* gene as internal control. The sequences of specific primers are presented in Table 2. A Biosystems 7500 Sequence Detection System (ABI, Foster City, CA, USA) was used for RT-qPCR analysis. After standardization with endogenous references, the $2^{-\Delta\Delta Ct}$ means was utilized to assess the relative mRNA and miRNA expression levels.

### 2.5. Proliferation of cervical cancer cells

The CCK-8 detection reagent was used in this study to detect the inhibitory influence of miR-9-5p on the proliferation of

**Table 2** Specific primer sequences applied to this study.

| Genes | Sequences |
|---|---|
| miR-9-5p | GGGGGAGCCAGGAAGTATTGA |
| | GATGCTCCAGAGAGGAAACCAG |
| BRCA1 | TTCACCCTCTGCTCTGGGTA |
| | TGGTCACACTTTGTGGAGACA |
| OCT1 | CCACTTTCCACCCTACGCA |
| | TGTTGCCATCTCCACTCT |
| GADD45 | AGAAGACCGAAAGCGACCC |
| | GTTGATGTCGTTCTCGCAGC |
| *gapdh* | ATGTTGCAACCGGGAAGGAA |
| | AGGAAAAGCATCACCCGGAG |

cervical cancer cells. All operations during the experiment followed the manufacturer's instructions with certain appropriate modifications (Hos et al., 2011). In brief, cervical cancer cells in the logarithmic growth period were obtained and seeded into 96-well culture plates at an ultimate density of 1 × $10^4$ cells per well. Then, the cells were incubated at 37 ℃ in 5% $CO_2$ humidified culture medium for 12 h. Subsequently, 20 mL of miR-9-5p mimics, miR-9-5p inhibitors, mimic control, and suppressor control, were transfected into cervical cancer cells with Lipofectamine™ 3000. After 48 h treatment, 10 μL CCK-8 reagent was mixed to every well, followed by another 2 h incubation. Finally, the absorbance (optical density) values of each well were estimated at a wavelength of 450 nm on an enzyme immunoassay analyzer (Bio-Rad, USA). The mimics and inhibitors of miR-9-5p and related controls were purchased from Thermo Fisher Scientific. The entire experimental procedure was repeated three times.

### 2.6. Oligonucleotide construction and cell transfection

To upregulate or downregulate the relative expression of miR-9-5p in the cervical cancer lesions or cervical cancer cells, miR-9-5p mimic, miR-9-5p inhibitor, mimic control, and inhibitor control were designed. All the oligonucleotides used in this research were synthesized by RiboBio (Guangzhou, China). The pIRES2-EGFP vector with BRCA1 cDNA fragment sequence and the negative control plasmids without miR-9-5p targeting sites in 3′-UTR were constructed by ShengGong Pharma (Shanghai, China).

The constructed plasmids and oligonucleotides were transfected into cervical cancer cells by applying Lipofectamine™ 3000 (Invitrogen, Carlsbad, CA, USA) on the basis of guidelines with a slight modification (Izsvák et al., 2009). Then, RT-qPCR assay was performed 24 h after transfection to determine transfection efficiency.

### 2.7. Luciferase reporter assays

Wild-type (WT) 3′-UTRs of BRCA1 that contained the predicted miRNA binding site of miR-9-5p and relevant mutant controls (MUT) without the miRNA binding site of miR-9-5p were reproduced into pMIR-REPORT luciferase reporter plasmids (Promega Corporation, Madison, WI, USA) under the guidance of the protocols (Li et al., 2013). Then, WT or MUT versions of BRCA1-3′-UTR and miR-9-5p oligonu-

cleotides were transfected into cervical cancer cells via Lipofectamine™ 3000. Cells were collected 48 h after transfection. Luciferase activities were evaluated by using a luciferase reporter assay system (E1980; Promega). Data were presented as mean ± standard deviation (SD). The entire experimental procedure was repeated three times.

### 2.8. Intravitreal injections of miRNA

Short hairpin RNA sequences of miR-9-5p were inserted into the pIRES2-EGFP vector and prepared into GV248 lentiviral particles for miR-9-5p silencing in vivo. The cervical cancer cells mice utilized in the study were randomly separated into four diverse groups and injected with miR-9-5p mimic, miR-9-5p inhibitor, mimic control, and inhibitor control. All injections were made directly after laser treatment, and intravitreal injections were manipulated following established protocols (Remole, 1989).

### 2.9. Flow cytometry analysis of apoptosis

An annexin V-fluorescein isothiocyanate (FITC) kit (KeyGen-Biotech, Nanjing, China) was used for the evaluation of the percentage of apoptotic cervical cancer cells after transfection with miR-9-5p mimic, miR-9-5p inhibitor, mimic control, and inhibitor control. All operations during the experiment followed the manufacturer's instructions with several appropriate modifications (Liu et al., 2016). In summary, cervical cancer cells were transplanted into six well plates and transfected with miR-9-5p oligonucleotides. Then, 5 μL of Annexin V-FITC and Propidium iodide (PI) solution was added to the well for 15 min at normal temperature in the dark. Then, after, the cells were directly evaluated via a BD FACSCalibur flow cytometry program (BD Biosciences, San Jose, CA, USA).

### 2.10. Enzyme-linked immunosorbent assay (ELISA) detection

miR-9-5p mimic, miR-9-5p inhibitor, mimic control, and inhibitor control were transfected into the cervical cancer cells mice or cervical cancer cells. The release level of the VEGF and PEDF contents in cervical cancer cells lesions or cell supernatant was evaluated via ELISA detection following the manufacturer's instructions with certain appropriate modifications (Ashrafi, 2014). This preformation was conducted more than three times, and data were reported as mean ± SD.

### 2.11. Statistical analyses

Statistical analysis of the data obtained from this research was performed using the commercial software SPSS 21.0 (SPSS, Chicago, IL, USA). This preformation was conducted more than three times, and the outcome was reported as mean ± SD. Students' *t*-test was adopted for the statistical comparison of two groups. One-way ANOVA was used for the statistical comparison of various groups. When the p value was $< 0.05$, the results were statistically significant

## 3. Results and discussion

### 3.1. Structural characterization

Pink block crystals of Complex **1** were created via the chemical change of Co(II) salt, $H_2$ppda, and pbmeix in a DMF aqueous solution at 120℃. It formed crystals in the triclinic space group *P*–1; and the asymmetric part produced a Co(II) center, a single ppda ligand, a pbmeix ligand, half an non-coordination pbmeix molecule, and a contained water molecule (Fig. 1a). The Co(II) ion was coordinated with double N atoms (N1 and N4$^{ii}$) from double various pbmeix ligands and double carboxylic acid O atoms (O1 and O3$^{i}$) from double various ppda ligands [(i) $-x + 2, -y + 1, -z + 1$) × [illegible], $y$, $z$]. In particular, it exhibited a crooked tetrahedral coordination structure ($\tau_4$ was 0.78), and the bond angles ranged from 95.76(8)° to 133.49(9)°. The ppda coordinated with the Co(II) center via the $\mu_2 - \kappa^1{:}\kappa^0{:}\kappa^1{:}\kappa^0$ coordination pattern, and the $CH_2CO_2$ groups of the ppda linker were crooked relative to one another in an anti-conformation. The Co(II) centers were linked with ppda ligands to construct 1D chains (Fig. 1b), and these chains were interconnected via pbmeix ligands to produce a 1D nanotubular framework in which coupled pbmeix ligands linked with double Co(II) ions to form $Co_2(pbmeix)_2$ 26-membered rings. The inclusive, non-coordinating pbmeix molecules were located in these nanotubes, with each $Co_2(pbmeix)_2$ ring pierced through by one pbmeix molecule (Fig. 1c). Notably, the imidazole rings of adjacent pbmeix molecules were parallel to each other, and the distance between them (3.547 Å) was extremely short. This condition was identical to π–π interaction. The adjacent 1D nanotube framework and the inclusive pbmeix and $H_2O$ molecules were linked via H-bond, C-H···π, and π···π interactions to form a 3D supramolecular framework (Fig. 1d).

To estimate the phase purity of the compounds, PXRD detection was conducted for these compounds (Fig. 2a). The apex of the study and simulated PXRD images were consistent with one another, illustrating that the crystal framework was an authentic member of the blocky crystal compounds (Chen et al., 2013). The difference in strength may be attributed to the quality of the sampled crystal. To learn the thermal decomposition procedure, TGA of **1** was conducted (Fig. 2b). When temperature ranged from 63℃ to 223℃, the coordinating water molecules of complex **1** gradually disappeared, and the percentage of mass reduction was 2.70%. Complex **1** began to disintegrate upon further warming, and the residues were oxides (CoO, found: 11.47%, calcd: 11.26% for 1).

### 3.2. Upregulated expression level of BRCA1 in cervical cancer cells mice

With regard to the important role of BRCA1 in different biological procedures, such as cell viability, adhesion, and mobility, RT-qPCR was performed in this experiment to detect the relative expression level of BRCA1 in the lesions of cervical cancer mice. Then, 7, 14, and 21 days after the construction of cervical cancer mice, the lesions were collected and normal rats were used as controls. As shown by the data in Fig. 3, the BRCA1 mRNA levels in the lesions of cervical cancer mice

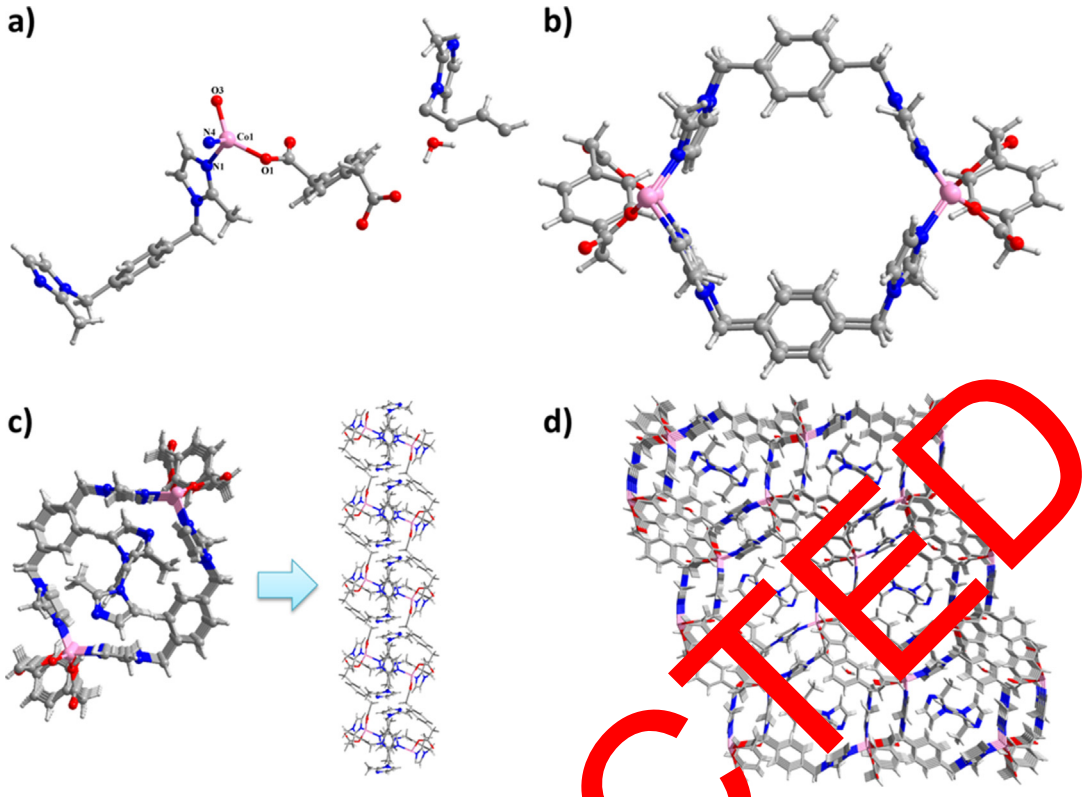


**Fig. 1** (a) Least building part of **1**. (b) 24 members of **1**. (c) View down the axis of a nanotube. (d) 3D supramolecular framework of **1**.

were considerably increased in contrast with those in normal tissues. The upregulated level of BRCA1 mRNA increased during the first 2 weeks, but decreased at the third week (Fig. 3A). The western blot results also indicated that the BRCA1 protein level in the lesions of the cervical cancer mice was increased during the first 2 weeks and decreased at the third week (Fig. 3B). The statistical analysis in Fig. 3B is illustrated in Fig. 3C.

### *3.3. Identification of miR-9-5p that directly targets BRCA1*

In our previous study, we concluded the abnormal expression level of BRCA1 in BRCA lesions, indicating the essential role of BRCA1 in the occurrence and growth of cervical cancer. However, determining how BRCA1 expression was regulated must still be explored. In this section, the Target Scan Human (http://www.targetscan.org/ vert_72/) software was used to evaluate the potential mRNA regulator of BRCA1 in the occurrence and development of cervical cancer. As displayed by the data in Fig. 4A, miR-9-5p was predicated as one of the most potential regulators of the miR-9-5p of BRCA1 in the occurrence and development of cervical cancer with the highest scores (A). Then, cervical cancer cells were co-transfected via miR-9-5p mimic, miR-9-5p inhibitor, simulation control, and inhibitor control. The related BRCA1 expression level was evaluated via RT-PCR. The result demonstrated

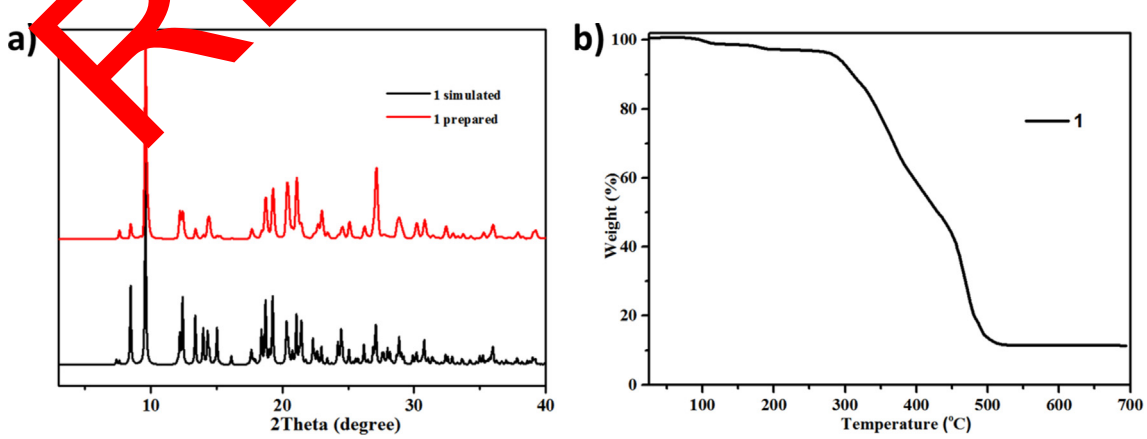


**Fig. 2** (a) PXRD images of **1**. (b) TGA curve of **1**.

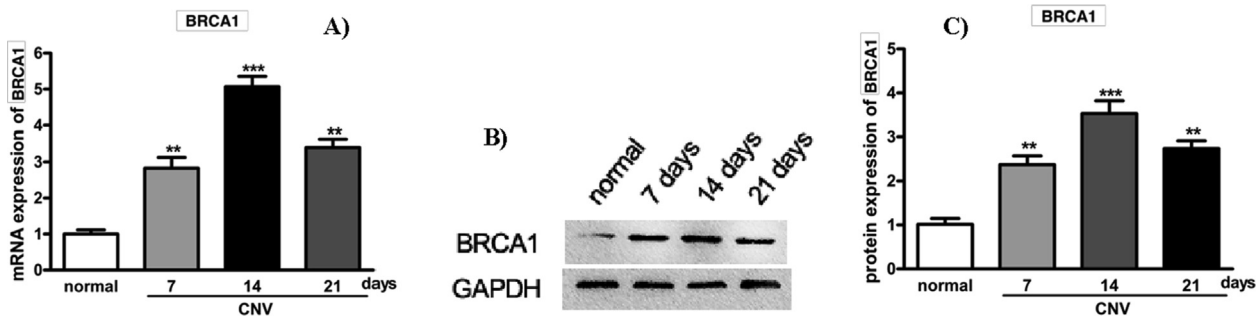


**Fig. 3** The expression level of BRCA1 in cervical cancer mice was upregulated. The cervical cancer mouse model was constructed, and the expression of BRCA1 was detected. RT-qPCR was performed to assess BRCA1 mRNA levels in the lesion at an indicated time (A). Western blot preformation was conducted for BRCA1 protein level evaluation (B). Statistical analysis of Fig. 3B (

that the miR-9-5p mimic can considerably restrain BRCA1 expression, and the miR-9-5p inhibitor evidently induced BRCA1 expression (B). Subsequently, the correlativity between miR-9-5p and BRCA1 was detected deeply. The results in Fig. 4C suggest that miR-9-5p expression can negatively regulate the expression level of BRCA1 in cervical cancer cells ($r = -0.9913$, $p < 0.0001$). The preceding results confirmed the negative regulation relationship between miR-9-5p and BRCA1, and the interaction between miR-9-5p and BRCA1 was deeply explored via luciferase reporter assay, as shown in Fig. 4D. The result suggested that miR-9-5p mimic considerably restrained luciferase activity and evidently elevated luciferase activity ($p < 0.005$). Moreover, we proved that miR-9-5p was the upstream of BRCA1 in cervical cancer cells, and this condition can negatively regulate BRCA1 relative expression.

### 3.4. miR-9-5p overexpression influences the proliferation and apoptosis of cervical cancer cells

As the upstream regulator of BRCA1, miR-9-5p has been proven to negatively regulate the relative expression of BRCA1 in

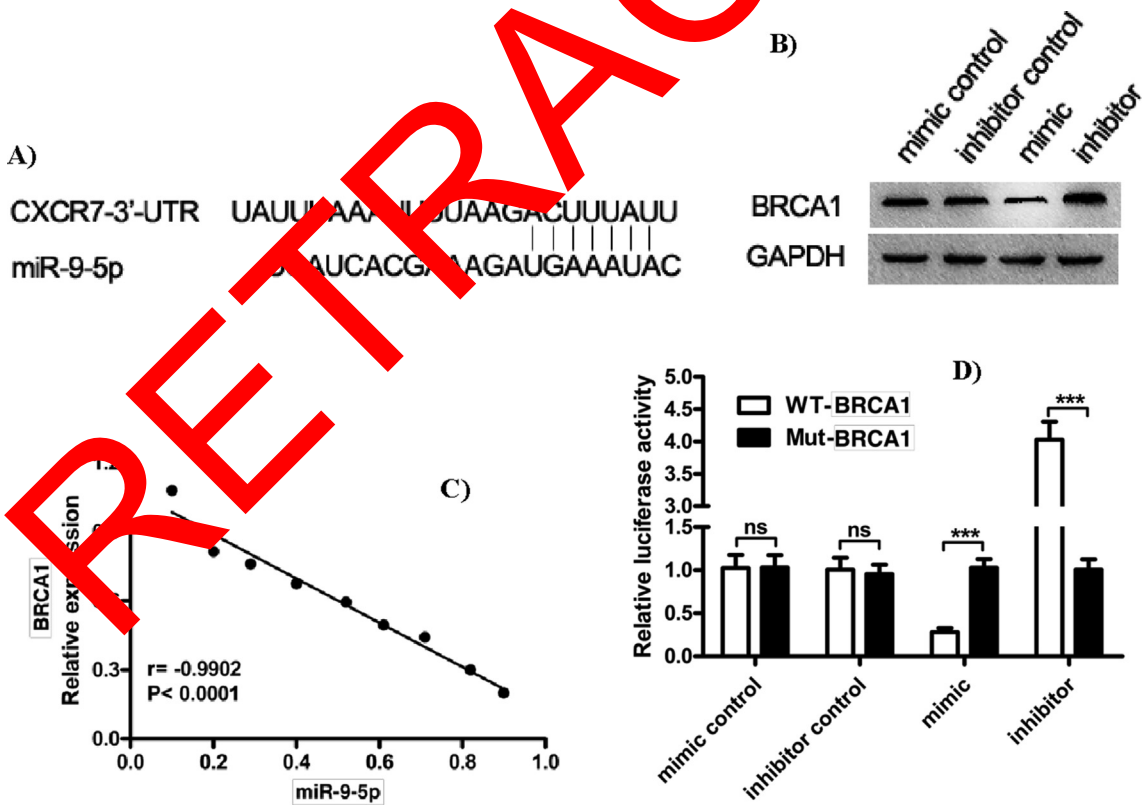


**Fig. 4** BRCA1 was negatively regulated by miR-9-5p in cervical cancer cells. Target Scan Human (http://www.targetscan.org/ vert_72/) software was used as the potential regulator of BRCA1 and the binding site on 3′-UTR (A). Influence of miR-9-5p transfection on the relative expression of BRCA1 in cervical cancer cells (B). SPASS analysis was conducted for the correlativity evaluation between miR-9-5p and BRCA1 (C). Luciferase reporter examination was performed to confirm the interactive combination between miR-9-5p and BRCA1 (D).

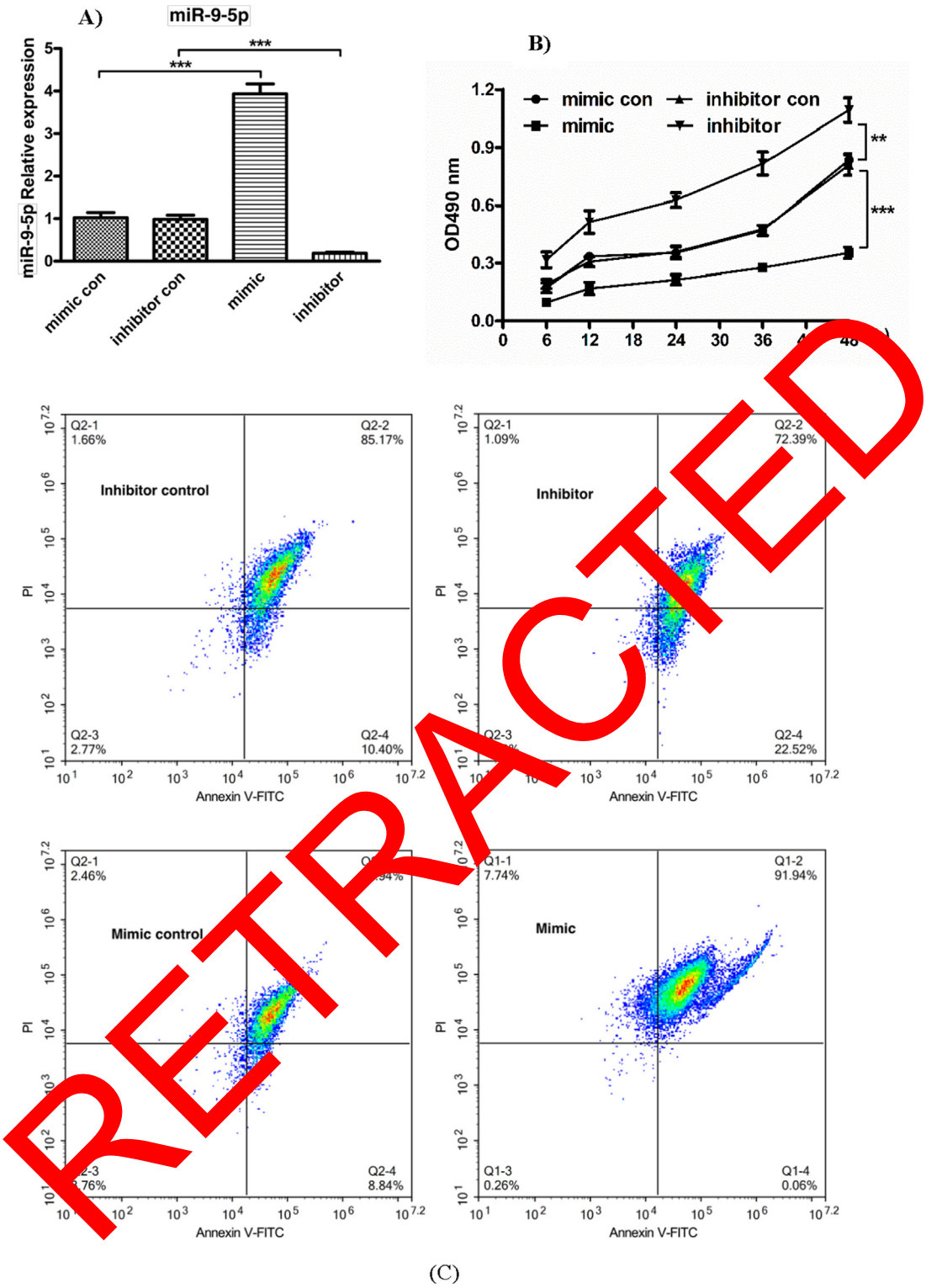


(C)

**Fig. 5** Inhibited proliferation and induced apoptosis of cervical cancer cells after miR-9-5p overexpression. cervical cancer cells were co-transfected by miR-9-5p mimic, miR-9-5p inhibitor, simulation control, and restrainer control. The relative expression of miR-9-5p after transfection was detected through RT-PCR (A). The viability of the transfected cervical cancer cells was determined via CCK-8 assay (B). The apoptosis of cervical cancer cells after transfection was determined through Annexin V-FITC/PI assay (C).

cervical cancer cells by directly combining with the 3′-UTR of BRCA1. Subsequently, the important biological role of miR-9-5p in the occurrence and growth of cervical cancer was further explored. First, the relative expression of miR-9-5p in cervical cancer cells after miR-9-5p co-transfection was measured via RT-PCR (Fig. 5A). Then, the inactive influence of miR-9-5p

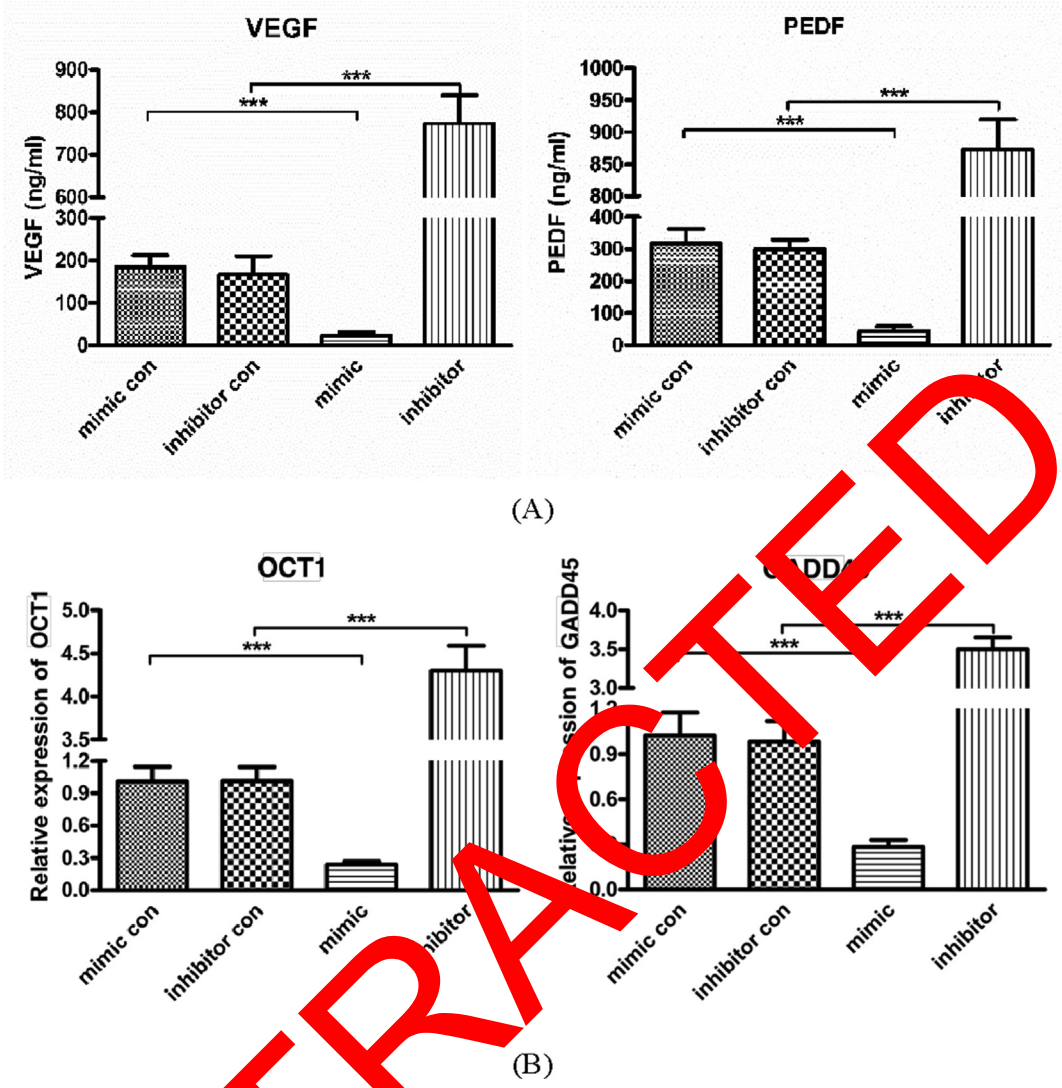




**Fig. 6** Suppressed OCT1 and GADD45 pathway activation by miR-9-5p/BRCA1. Cervical cancer cells were co-transfected by miR-9-5p mimic, miR-9-5p inhibitor, the simulation control, and restrainer control. The release of VEGF and PEDF was estimated using an ELISA detection kit (A). The relative expression of the GADD45 and OCT1 in cervical cancer cells was determined via RT-PCR.

on cervical cancer cells. Cell proliferation was evaluated through CCK-8 assay. As shown in Fig. 5B, miR-9-5p mimic transfection can significantly reduce the proliferation of cervical cancer cells in contrast with the mimic control group. Compared with this result, the proliferation of cervical cancer cells was evidently increased after miR-9-5p inhibitor transfection (Fig. 5B). Second, annexin V-FITC/PI assay was conducted, and the result demonstrated a considerably higher level of apoptotic cervical cancer cells after miR-9-5p mimic transfection; moreover, the apoptosis of cervical cancer cells was significantly decreased after transfection with miR-9-5p (Fig. 5C). Furthermore, miR-9-5p mimic enhanced cell viability and reduced cell apoptosis in cervical cancer cells.

### *3.5. miR-9-5p suppresses OCT1 and GADD45 pathways by targeting BRCA1*

In this section, we identified the specific mechanism of the occurrence and development of cervical cancer mediated by miR-9-5p/BRCA1. As previously reported, VEGF and PEDF can stimulate neovascularization, and a combined increased level of VEGF and PEDF is typically observed in cervical cancer. Thus, the contents of VEGF and PEDF after miR-9-5p oligonucleotide transfection were assessed using an ELISA detection kit. As indicated in Fig. 6A, the miR-9-5p mimic considerably restrained the levels of the VEGF and PEDF. Moreover, downstream responders of VEGFR2, such as GADD45 and OCT1, may play complex roles in controlling angiogenesis and vascular permeability. They may also be important for the occurrence and development of cervical cancer. Our findings showed that after co-transfected by miR-9-5p mimic, the relative expression levels of GADD45 and OCT1 were considerably decreased in contrast with those of the mimic control group. Furthermore, miR-9-5p inhibitor transfection can evidently increase GADD45 and OCT1 levels in cervical cancer cells (Fig. 6B). All the results demonstrate that miR-9-5p restrains the OCT1 and GADD45 pathways by controlling BRCA1.

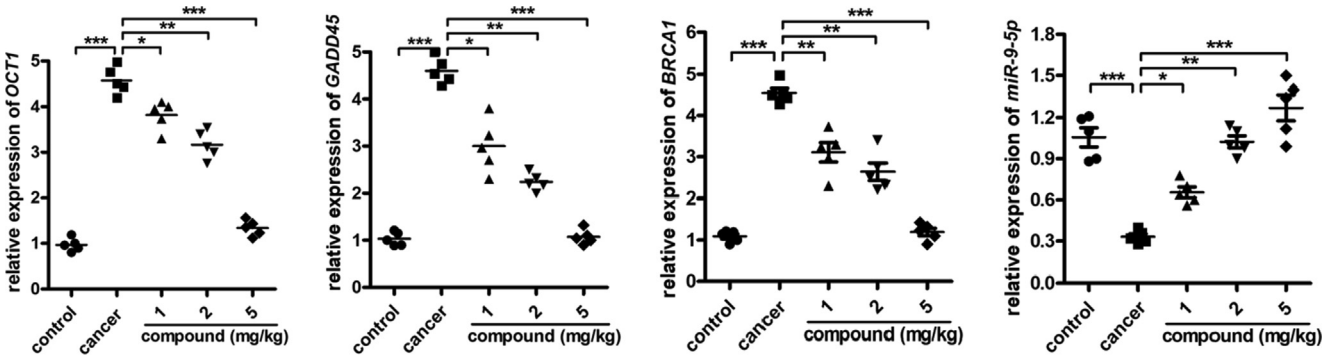


**Fig. 7** Regulated OCT1 and GADD45 pathway activation via miR-9-5p/BRCA1 after injection. The cervical cancer animal model was constructed, and the compound was injected at concentrations of 1, 2, and 5 mg/kg. The relative expression of miR-9-5p, BRCA1, OCT1, and GADD45 was estimated via RT-qPCR.



### *3.6. Regulation of complex 1 on OCT1 and GADD45 pathway activation via miR-9-5p/BRCA1*

After the design and synthesis of complex **1**, its application values in cervical cancer treatment were determined. In Fig. 4, we e proved that after co-transfection with miR-9-5p mimic, the relative expression levels of GADD45 and OCT1 were considerably decreased in contrast with those of the mimic control model. In addition, miR-9-5p inhibitor transfection can evidently increase GADD45 and OCT1 levels in cervical cancer cells. Thus, after the exposure of complex **1**, RT-qPCR was exhaustively performed to determine OCT1 and GADD45 pathway activation and miR-9-5p/BRCA1 expression levels. The data in Fig. 7 illustrate a diminished level of miR-9-5p and increased levels of BRCA1, OCT1, and GADD45 in the cervical cancer model group. After the treatment of complex **1**, the expression level of miR-9-5p was upregulated and the levels of BRCA1, OCT1, and GADD45 were reduced significantly. The biological activity of complex **1** also exhibited a dose-dependent relationship.

## 4. Conclusion

The important role of miRNA in regulating a variety of target proteins involved in cervical cancer generation has been identified through the long-term exploration of the pathogenesis of cervical cancer. In the present research, we first estimated the important role of BRCA1 in the occurrence and development of cervical cancer. Subsequently, miR-9-5p was assumed as a potential novel regulator of BRCA1 expression that can bind to the 3′-UTR of BRCA1. The direct binding of miR-9-5p and BRCA1 in cervical cancer cells was further evaluated via luciferase activity assay. In the biological functional research, the inactive influence of miR-9-5p on cervical cancer cells proliferation was detected via CKK-8 assay. The data indicated that miR-9-5p mimic can considerably diminish the proliferation of cervical cancer cells compared with that in the control group. By contrast, miR-9-5p inhibitor exerts an opposite promotion effect on cervical cancer cell proliferation. Consistent with this result, the VEGF and PEDF released by cervical cancer cells were also reduced after miR-9-5p mimic transfection. In the molecular mechanism investigation, the OCT1 and GADD45 pathways were proven to be regulated by miR-9-5p overexpression. In addition, a new Co(II) complex was designed and synthesized. This complex was proven to have excellent application values in cervical cancer therapy by regulating miR-9-5p, BRCA1, OCT1, and GADD45 in cervical cancer cells. However, research in this area is still in its early stages, and many issues remain to be solved. For example, how do specifically expressed miRNA play one-to-many regulatory roles in various types of cells in the cervical cancer microenvironment and interact with other signaling pathways? How can they be changed without affecting the cervical cancer? Does MiRNA inhibit the growth of pathological neovascularization in the cervical cancer? At present, inhibitors or mimics of miRNA have been reported to upregulate or downregulate the expression of miRNA in cancer tissues and then regulate the expression of protein-encoding genes, eventually achieving the objective of treating diseases. This scenario is also an important direction for future research. With the deepening of such research, the elucidation of miRNA mechanism can provide a new targeted treatment of cervical cancer.

## Funding

The research was supported by the Scientific Research Project of Hunan Provincial Health Commission in 2021 (202105012363).

## References

Wuerthner, B.A., Avila-Wallace, M., 2016. Cervical cancer: Screening, management, and prevention. Nurse Pract. 41, 18–23.

Fang, J., Zhang, H., Jin, S., 2014. Epigenetics and cervical cancer: from pathogenesis to therapy. Tumour Biol. 35, 5083–5093.

Tsikouras, P., Zervoudis, S., Manav, B., Tomara, E., Iatrakis, G., Romanidis, C., Bothou, A., Galazios, G., 2016. Cervical cancer: screening, diagnosis and staging. J BUON 21, 320–325.

Harao, M., Ando, J., Kamata, H., Hoshi, N., Igarashi, S., Sekiguchi, R., Sugano, K., 2018. Peritoneal cancer arising after total abdominal hysterectomy and bilateral salpingo-oophorectomy for cervical cancer in a patient with right breast cancer and germline mutation of BRCA1 gene: a case report and literature review. Breast Cancer 25, 243–249.

Xu, G.P., Zhao, Q., Wang, D., Xie, W.Y., Zhang, L.J., Zhou, H., Chen, S.Z., Wu, L.F., 2018. The association between BRCA1 gene polymorphism and cancer risk: a meta-analysis. Oncotarget 9, 8681–8694.

Amini, S., Abak, A., Sakhinia, E., Abhari, A., 2019. MicroRNA-221 and MicroRNA-222 in Common Human Cancers: Expression, Function, and Triggering of Tumor Progression as a Key Modulator. Lab Med. 50, 333–347.

Laengsri, V., Kerdpin, U., Plabplueng, C., Treeratanapiboon, L., Nuchnoi, P., 2018. Cervical Cancer Markers: Epigenetics and microRNAs. Lab Med. 49, 97–111.

Shen, S., Zhang, S., Liu, P., Wang, J., Du, H., 2020. Potential role of microRNAs in the treatment and diagnosis of cervical cancer. Cancer Genet. 248–249, 25–30.

Liu, J.J., Xia, S.B., Duan, Y.L., Liu, T., Cheng, F.X., Sun, C.K., 2018. Anion-Controlled Architecture and Photochromism of Naphthalene Diimide-Based Coordination Polymers. Polymers (Basel) 10, 165.

Raja, D.S., Bhuvanesh, N.S.P., Natarajan, K., 2012. A novel water soluble ligand bridged cobalt(ii) coordination polymer of 2-oxo-1,2-dihydroquinoline-3-carbaldehyde (isonicotinic) hydrazone: evaluation of the DNA binding, protein interaction, radical scavenging and anticancer activity. Dalt. Trans. 41, 4365–4377.

Hu, X.G., Li, X., Yang, S.I., 2015. Novel photochromic infinite coordination polymer particles derived from a diarylethene photoswitch. Chem. Commun. 51, 10636–10639.

Castro, M.R., Lutz, D., Edelman, J.L., 2004. Effect of COX Inhibitors on VEGF-induced Retinal Vascular Leakage and Experimental Corneal and Choroidal Neovascularization. Exp. Eye Res. 79, 275–285.

Qian, Y.Y., Wu, H.Y., Liu, G.Q., Ren, C., Lu, P.R., Zhang, X.G., 2019. Blockade of Insulin Receptor substrate-1 Inhibits Biological Behavior of Choroidal Endothelial Cells. Int. J. Ophthalmol. 12, 1386–1394.

Hos, D., Regenfuss, B., Bock, F., Onderka, J., Cursiefen, C., 2011. Blockade of Insulin Receptor substrate-1 Inhibits Corneal Lymphangiogenesis. Invest. Ophthalmol. Vis. Sci. 52, 5778–5785.

Izsvák, Z., Chuah, M.K.L., Vandendriessche, T., Ivics, Z., 2009. Efficient Stable Gene Transfer Into Human Cells by the Sleeping Beauty Transposon Vectors. Methods 49, 287–297.

Li, H., Wang, Y., Cao, F., 2013. In Vivo Bioluminescence Imaging Monitoring of Stem Cells' Participation in Choroidal Neovascularization. Ophthalmic. Res. 50, 19–26.

Remole, A., 1989. Anisophoria and Aniseikonia: Part I. The Relation Between Optical Anisophoria and Aniseikonia. Optom. Vis. Sci. 66, 659–670.

Liu, X., Zhu, M., Yang, X., Yang, J., Qin, B., Gu, C., Chen, H., Sang, A., 2016. Inhibition of RAC1 Ameliorates Choroidal Neovascularization Formation in Vitro and in Vivo. Exp. Mol. Pathol. 100, 451–45.

Askou, A.L., 2019. Development of Gene Therapy for Treatment of Age-Related Macular Degeneration. Acta Ophthalmol. 92, 1–38.

Chen, N., Li, M., X., Yang, P., Sun, X., Shao, M., Zhu, S.-R., 2013. Chiral Coordination Polymers with SHG-Active and Luminescence: An Unusual Homochiral 3D MOF Constructed from Achiral Components. Cryst. Growth Des. 13, 2650–2660.